Wrinkling Prediction Procedure in Thin Sheet Metal Forming Processes with Adaptive Mesh Refinement

Part II : Wrinkling with contact

Project Title	Modelling of Sheet Metal Forming
Project Number	ME97033
Cluster	Modelling of Forming of Metal and Laminate Products
Author	A. Selman University of Twente Netherlands Institute *for* Metals Research
Project Leaders	A.H. van den Boogaard
Cluster co-ordinator	J. Huetink

October 2001

Contents

1. Introduction

In a numerical simulation, wrinkles can be detected by a visual inspection of the deformed mesh. However, this implies that the finite element mesh used is fine enough to allow a proper capture of the wrinkles. This, in general, makes it cumbersome to proceed with the analysis. Rather, it is desirable to proceed with a selective refinement to keep the computational cost low (acceptable). Whenever the mesh needs to be modified, it is generally not necessary to reconstruct the whole mesh but only to modify it locally using mesh densities based on *wrinkling indicators* from the previous mesh.

Furthermore, in designing optimal forming tools it is desirable that wrinkle formation tendencies can be assessed at a low computational cost at an early stage of the simulation, so that, if necessary, it can be stopped and started over again from the beginning with a new design.

In sheet metal forming numerical simulations it is important to create and maintain appropriate meshes. In this context, the use of discretisation error estimation in connection with adaptive mesh refinement plays an essential role *(NIMR Publication : P.00.1.022)*. However, to answer a frequently asked question, when wrinkling takes place the discretisation errors estimator is generally not able to detect the initiation of wrinkling nor it can capture shallow wrinkling. It will only spot wrinkles when large rotations develop, at which stage it is too late to proceed with a mesh refinement. Therefore, it is necessary to develop separate wrinkling prediction tools to tackle this problem.

In part I of the present project *(NIMR Publication : P.00.1.016)* we have concentrated our attention on contact free wrinkling prediction based on Hutchinson analysis.
We considered a doubly curved sheet element with principal radii of curvature and thickness assumed to be constant over the region of the sheet being examined for susceptibility to wrinkling.
Simplifications did arise from the fact that the anticipated short-wavelength modes are shallow and can be analysed using Donnell-Mushtari-Vlasov (DMV) shallow shell theory.
We also assumed that the stress state prior to wrinkling to be a uniform membrane state and, for simplicity, that the principal directions of the uniform membrane stress state coincide with the principal axes of curvature.
We could under these assumptions, limitations and simplifications obtain a simple wrinkling criterion with some restrictive applicability. Nonetheless, the results were used to locally define a wrinkling risk factor or simply a wrinkling indicator, which in turn, was used to detect the zones (elements) to be refined in a subsequent adaptive mesh refinement process. To complete the analysis, the wave length number was used to determine the appropriate new mesh size (please refer to Part I of this report).

When contact is taken into account the problem is further complicated and no simple criterion can be expected.

Furthermore, given that numerical simulations of complex sheet metal forming involve large scale models, it is obvious that global wrinkling indicators found in the literature - mostly based on eigen value analysis of the global tangent stiffness matrix - should not be

used because of their high computational cost. This is to avoid over-loading the already time consuming deep drawing simulations. Consequently, a method based on local indicators, such as the one presented by Per Nordlund (1997) looks very attractive and was in our view worth implementing.

Nordlund's approach stems from the fact that the formation of wrinkles is characterised by the occurrence of areas where the deformation is dominated by strong out of plane rotations. The algorithmic procedure presented by P. Nordlund is based on the local value of the second order increment of internal work for capturing the initiation of wrinkling. Evaluated element wise, it gives an indication when becoming negative to when and where wrinkles start to grow. It requires no assumptions about shapes of wrinkles and handles contact conditions without extra manipulation.

The wrinkling analysis as presented by P. Nordlund, is now briefly described.

2. Wrinkling analysis

An important observation in wrinkling prediction context is that the formation of wrinkles is characterised by the occurrence of areas where the deformation is dominated by strong local out of plane rotations. This behaviour can be traced by following the evolution of a scalar quantity namely the second-order increment of internal work which is given, in a matrix format, by

$$I = \int_V tr\left\{(\dot{\sigma} + tr(\mathbf{L})\,\sigma - \mathbf{L}\,\sigma)\mathbf{L}\right\}\mathrm{dV} = \int_V \dot{\mathbf{f}}^{\mathrm{b}}\mathbf{v}\,\mathrm{dV} + \int_{S_t} \dot{\mathbf{f}}^{\mathrm{s}}\mathbf{v}\,\mathrm{dS} \tag{1}$$

where $tr\{\ \}$ is the trace operator and $\mathbf{L} = grad(\mathbf{v})$ the velocity gradient tensor. Other terms are the well know Cauchy stress and its rate, the body and surface loads rates.

For physical interpretation, the Jaumann stress rate $\hat{\tau}$ of the Kirchhoff stress tensor $\tau = J\sigma$, is introduced

$$\hat{\tau} = \dot{\sigma} + tr(\mathbf{D})\sigma - \mathbf{W}\,\sigma - \sigma\,\mathbf{W}^T \tag{2}$$

where $\mathbf{D}$ and $\mathbf{W}$ are the symmetric and anti-symmetric parts of the velocity gradient tensor, respectively. $\mathbf{D}$ is usually called the rate of deformation tensor and $\mathbf{W}$ the body spin tensor.

Inserting (2) into (1) gives the following expression for the second-order increment of internal work

$$I = \int_V tr\left\{\hat{\tau}\,\mathbf{D} + \sigma(-\mathbf{D}\mathbf{D}^T + \mathbf{D}\mathbf{W} + \mathbf{W}^T\mathbf{D} + \mathbf{W}\mathbf{W}^T)\right\}\mathrm{dV} \tag{3}$$

Nordlund's approach consists of computing the scalar I over local regions of the structure. In particular the local regions are chosen to consist of finite elements. Potential areas for wrinkles will be found where this quantity becomes negative.

3. Nordlund's wrinkling indicator

At this stage there is a need to introduce a scaling that makes it possible to define a wrinkling indicator that always takes values in the interval $[-1,1]$.

I is split according to

$$I = I_{01} + I_{02} + I_{03} \tag{4}$$

where

$$I_{01} = \int_{V^{elem}} tr\left\{ \hat{\tau}\, \mathbf{D} + \sigma(-\mathbf{D}\mathbf{D}^T) \right\} \mathrm{dV} \tag{5}$$

$$I_{02} = \int_{V^{elem}} tr\left\{ \sigma(\mathbf{D}\mathbf{W} + \mathbf{W}^T\mathbf{D}) \right\} \mathrm{dV} \tag{6}$$

$$I_{03} = \int_{V^{elem}} tr\left\{ \sigma(\mathbf{W}\mathbf{W}^T) \right\} \mathrm{dV} \tag{7}$$

The following wrinkling indicator, is then defined

$$\bar{I}_{elem} = \frac{I_{01} + I_{02} + I_{03}}{|I_{01}| + |I_{02}| + |I_{03}|} \tag{8}$$

From the definition in (8), it is observed that $\bar{I}_{elem}$ satisfies the relation $|\bar{I}_{elem}| \le 1$.
Therefore,

- When the incremental displacement is dominated by the body spin

$$\bar{I}_{elem} \to \frac{I_{03}}{|I_{03}|} = \pm 1 \tag{9}$$

  where the minus sign is valid for a buckling situation (compressive membrane stresses).

- When the incremental displacement is dominated by the rate of deformation tensor

$$\bar{I}_{elem} \rightarrow \frac{I_{01}}{|I_{01}|} = 1 \tag{10}$$

4. Results and discussion

Per Nordlund's wrinkling indicator has been implemented and tested on a number of numerical examples.

A first test has been carried out on a simple pin jointed bar (Figure 1a). The exact results were obtained for this example as the solution actually follows the load-displacement curve.
It should be stressed here that the couple of bars are rotating under compressive stresses.
The same observations stand for the Euler beam example (Figure 1b) that is treated in details in Nordlund's publication.

Another situation where Nordlund's indicator gives good results, is in deep drawing simulations, in the part of the sheet under the blank holder. When the blank holder force is low to very low, or when a (large) gap is set between the blank holder and the die, large wrinkles (rotations) develop under strong compressive stresses.
Such situations are very much in favour of a good wrinkling indication by Nordlund's indicator.

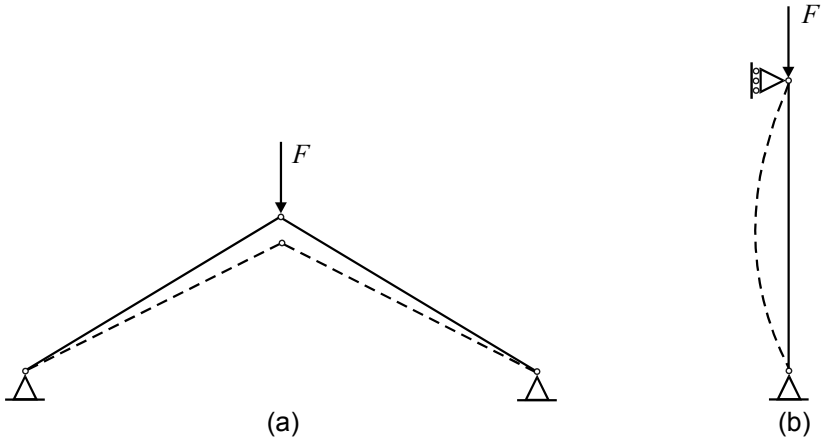

Figure 1 : (a) Pin-jointed structure and (b) Euler beam.

Next, Nordlund's indicator was tested on the hemispherical product that has been used to test the contact free wrinkling indicator based on Hutchinson's approach in part I of the present project. A high blank holder force was then used to avoid wrinkling under the blank holder as Hutchinson's approach covers contact free wrinkling only. Given the set of

geometric and material parameters used, wrinkling did occur in the hemispherical part of the product. Although the wrinkles were shallow with a rather large wave length, the Hutchinson's approach based wrinkling indication was good, and could be used, to drive a successful adaptive mesh refinement.

However, when Nordlund's indicator was tested on that very same example, it did not give the expected results *i.e.* no clear indication of the wrinkles was obtained. What was a clear picture with Hutchinson's approach became a blur picture, and could not be used to drive the adaptive mesh refinement. Different meshes, ranging from coarse to very fine, were used to see if that was not the cause of the poor indication and much efforts were also devoted to check the formulation and debug the code. Still, the results were not satisfactory.

To determine the cause(s) of the poor indication, the I_{03} indicator, which plays the dominating role when wrinkling takes place, was split into two parts :

- A first part that takes into account only the rotation and strain rates and stresses in the minor principal direction, and
- A second part that takes into account only the rotation and strain rates and stresses in the major principal direction.

The idea behind this split is to consider the principal directions separately in the hope that the compressive direction (alone) will show a better indication for wrinkling. In fact, this brings the case to a 1-D problem, which can be better apprehended.
Recall that in the formulae developed in Section 3, speaking in terms of principal stresses and rotations, both directions are taken into account. That is to say, if an element is under both compressive and tensile stresses, these play a challenging role in the determination of the wrinkling indicator. Note, that this is not the case in Hutchinson's approach, as the principal directions are considered separately.
The result of this attempt was a slight improvement in the compressive direction indication, but unfortunately, was not good enough to be used as such.

The whole exercise, although not successful in improving the results, allowed us by looking closely at all data, to find out, again for this particular example, that the change in rotations (during a single deep drawing step) is small to very small and that the compressive stresses that are already one order lower than the tensile stresses in the wrinkling zones, do relax at the initiation of wrinkling.

Now, looking back at Nordlund's indicator, when wrinkling occurs, the indicator will be, as stated above, mainly driven by

$$I_{03} = \int_{V^{elem}} tr\left\{ \sigma(\mathbf{W}\mathbf{W}^{T}) \right\} \mathrm{dV} \tag{11}$$

which is the product of the stresses and the related change in rotations. Therefore, when the rotations are small and squared, the result is that I_{03} tends to zero, whereby the global indicator will either approach the zero value else go slightly positive and consequently cannot be used to properly depict the formation of wrinkles.

Other tests were performed and the same conclusions were drawn.

The experience gained so far, was used to find another way of defining the wrinkling indicator.

5. A new wrinkling indicator

As already stated above, one of the causes of the poor indication of Nordlund's indicator is that the rotations are small in a *shallow wrinkling* situation and that these are squared in the formulae used.
This prompted us to use the curvatures in the design of an indicator. More precisely, to look at the change of curvatures (during a single deep drawing step) under compressive stresses. By doing so, all changes in curvatures that are not due to compressive stresses, such as those caused for example by the geometry of the tool and the die, are filtered out. These, however, will be taken into account by the (geometric) error estimation indicator if and when necessary. That is when the wrinkling prediction routine is used in conjunction with the adaptive mesh refinement routine.

The new wrinkling indicator in the i-principal direction is defined as

$$e_i^w = \frac{1}{A}\int \frac{R_i^t - R_i^{t+\Delta t}}{R_i^t R_i^{t+\Delta t}} dA \qquad i = 1,2 \tag{12}$$

with i representing the principal curvature (stress) [*] direction.

Note that we do consider the principal directions (stress and curvature) one at a time as is the case with Hutchinson's approach, and take the maximum change for each element. Consequently, the wrinkling indicator value e^w is defined as the maximum of e_i^w, *i.e.*

$$e^w = max\left| e_i^w \right| \qquad i = 1,2 \tag{13}$$

It should be stressed here, that the change of the curvature in a given direction is considered in the same direction as for the compressive stress and not in the perpendicular direction as is the case with Hutchinson's approach in the determination of critical stresses (strains).

[*] As for Hutchinson's approach, we consider that the principal stress and curvature directions do coincide.

Finally, we note that the present indicator can be viewed as a generalisation of the discretisation error indicators in which a (relative) change, *e.g.* in the thickness or geometry, is measured between the finite element solution and a higher order solution obtained by some solution recovery technique. The change in the solution for the wrinkling indicator is evaluated between the solution at the beginning and the end of a given deep drawing step, considering only elements under compressive stresses in the 1 and/or 2 principal directions.

As for Hutchinson's approach, the present indicator is local and is of a post-processing type, and is therefore determined at a very low cost.

6. Adaptive strategy

In the adaptive procedure we need to detect the zones (elements) to be refined and determine a new mesh size for those zones (elements). The zones detection is obtained by the use of the wrinkling indicator (13) and the new mesh size is obtained by the use of the following formula

$$L^w = L \, \frac{e^{avr}}{e^w} \tag{14}$$

where e^{avr} is the average value of e^w over all rotating elements and L the old element size.

Moreover, to avoid excessive refinement, a check against a user specified minimum size is to be operated before the refinement actually takes place.

The general algorithm for wrinkling prediction is presented in Figure 2.

At a given step N loop over all elements to

- Input all necessary data at the beginning and at the end of step N
- Evaluate the principal curvatures and their direction at the end of step N
- Determine the principal stress directions at the end of step N
- Check if curvature swap is necessary (See the Appendix)
- Evaluate the curvatures at the beginning of step N
- Compute the relative change in the curvature and the wrinkling indicator
- Determine the new mesh size

Figure 2 : General Algorithm for wrinkling prediction.

7. General comments

- The new routine has been tested on the hemispherical product, using a fine uniform mesh. The contour plots of the new indicator showed proper indication of the zones where wrinkling takes place. The indication is clear, and unlike the one obtained with Per Nordlund's indicator, can be used to drive subsequent mesh refinements. Numerical examples can be found in forthcoming publications devoted to *comprehensive approach to wrinkling prediction analysis*.

- It should be stressed that unlike the contact free wrinkling indicator, which can give a prediction before wrinkling actually takes place, the present indicator, as Per Nordlund's indicator, would give an indication only when the sheet starts to rotate under compressive stresses. It is therefore essential to capture the formation of wrinkles at their initiation. However, given that the computational cost to run the wrinkling indicator is very low, it is recommended to call the wrinkling indicator routine as often as necessary, especially at the beginning of the drawing process.

- The present indicator can of course be used in a contact free situation. However, because of the completeness that Hutchinson's approach provides, we prefer to use the new wrinkling indicator to complete Hutchinson's analysis based wrinkling indicator rather than a substitute to it.

- In part I of the report on wrinkling prediction the curvature evaluation has been presented in Appendix 3, and will not be repeated here. However, the determination of the principal stress directions along with the principal curvature directions has been added to the present report, and should also apply to part I of the report. The reason for this (necessary) addition is given in the appendix that is presented at the end of the present report.

8. References

P. Nordlund and B. Haggblad
Prediction of wrinkle tendencies in explicit sheet metal forming simulations
Int. J. Num. Meth. Eng., 40, 4079-4095, (1997).

P. Nordlund
Adaptivity and wrinkle indication in sheet metal forming
Comput. Methods Appl. Mech. Engrg. 161, 127-143, (1998).

J.W. Hutchinson
Plastic buckling
Adv. Appl. Mech., 14, 67-144 (1974).

J.W. Hutchinson and K.W. Neale
Wrinkling of curved thin sheet metal
Plastic Instability, J. Salencon (Ed.), Press Ponts et Chaussees, 71-78, (1985).

K.W. Neale
Numerical analysis of sheet metal wrinkling
Numiform ’89, Thompson et al (Eds.), 501-505, Balkema, Rotterdam, (1989)

K.W. Neale and P. Tugcu
A numerical analysis of wrinkling formation tendencies in sheet metals
Int. J. Num. Meth. Eng., 30, 1595-1608, (1990).

H. Ameziane-Hassani and K. Neale
On the analysis of sheet metal wrinkling
Int. J. Mech. Sci., 33, 13-30, (1991).

J.L. Batoz and G. Datt
Modelisation des structures par elements finis
Volume 3 : Coques
Hermes, Paris, 1990.

A. Selman
Notes on error estimation and adaptive mesh refinement in thin sheet metal forming processes
Netherlands Institute *for* Metals Research Publication : P.00.1.022 (2000).

A. Selman
Wrinkling prediction procedure in thin sheet metal forming processes with adaptive mesh refinement – Part I : Contact free wrinkling
Netherlands Institute *for* Metals Research Publication : P.00.1.016 (2000).

A. Selman, T. Meinders , A.H. van den Boogaard and J. Huetink
Wrinkling prediction with adaptive mesh refinement
3rd ESAFORM Conference on Material Forming, Stuttgart, 11-14 April, (2000).

Appendix to Part I and II

It is assumed in Hutchinson's approach that the principal directions of stress and curvature do coincide.
With reference to the critical stress (strain) formulae used in the contact free wrinkling report (Part I), it is clear that for instance, to determine the critical stress (strain) in the 1-direction, the radius of curvature in the opposite direction i.e. the 2-direction is to be used.
A problem arises when the principal curvature in the first direction coincides with the second principal direction of stresses (strains) and not with the first. Therefore, it is necessary to find out, prior to the evaluation of the critical stress (strain) values, the correct radius of curvature to be used.
It is the aim of the present additional notes to explain how this problem has been dealt with and programmed.
First the principal curvature directions are determined, then the principal stress directions are found. Finally, a dot product between the first directions of stress (strain) and curvature is performed to check if a swap of the radii of curvatures is necessary.

The same adjustments have to be made in the new wrinkling indicator (Part II) as we need to know which radius of curvature is actually in the direction of the compressive stress.

Principal curvature directions [1]

Consider again equation (A3-3) of Appendix 3 (Part I) (See also Figure A1 to A3)

$$[b]\begin{bmatrix} 1 \\ \lambda \end{bmatrix} - \frac{1}{R}[a]\begin{bmatrix} 1 \\ \lambda \end{bmatrix} = \begin{bmatrix} 0 \\ 0 \end{bmatrix} \tag{A1}$$

Substitute $\frac{1}{R}$ in the above equation by

$$\frac{1}{R} = \frac{II}{I} = \frac{b_{11} + 2b_{12}\lambda + b_{22}\lambda^2}{a_{11} + 2a_{12}\lambda + a_{22}\lambda^2} \tag{A2}$$

where I and II are the first and second fundamental forms of a given surface A, respectively.
Using the first line of equation (A1), the following expression is obtained

$$d^2\eta\,(a_{12}b_{22} - a_{22}b_{12}) + d\xi\,d\eta\,(a_{11}b_{22} - a_{22}b_{11}) + d^2\xi\,(a_{11}b_{12} - a_{12}b_{11}) = 0 \tag{A3}$$

in which the ratio $\lambda = d\eta / d\xi$ has been introduced.

[1] J.L. Batoz and G. Datt
Modelisation des structures par elements finis Volume 3 : Coques, Hermes, Paris, 1990.

Equation (A3) is equivalent to

$$\begin{vmatrix} d\eta^2 & -d\xi\, d\eta & d\xi^2 \\ a_{11} & a_{12} & a_{22} \\ b_{11} & b_{12} & b_{22} \end{vmatrix} = 0 \qquad \text{(A4)}$$

Using $d\eta = \lambda\, d\xi$ in (A3) and simplifying by $d^2\xi$, we obtain the following equation

$$\lambda^2 (a_{12}b_{22} - a_{22}b_{12}) + \lambda (a_{11}b_{22} - a_{22}b_{11}) + (a_{11}b_{12} - a_{12}b_{11}) = 0 \qquad \text{(A5)}$$

Let λ_1 and λ_2 be the roots of the above equation.

The normality condition of the principal directions gives

$$[d\xi_i\, , d\eta_i][a]\begin{bmatrix} d\xi_j \\ d\eta_j \end{bmatrix} = \delta_{ij} \qquad (i, j = 1,2) \qquad \text{(A6)}$$

that is

$$d\xi_i d\xi_j a_{11} + d\xi_j d\eta_i a_{21} + d\xi_i d\eta_j a_{12} + d\eta_j d\eta_i a_{22} = \delta_{ij} \qquad (i, j = 1,2) \qquad \text{(A7)}$$

Consider $i = j = 1$ in (A7)

$$d\xi_1^2\, a_{11} + 2\, d\xi_1 d\eta_1\, a_{12} + d\eta_1^2\, a_{22} = 1 \qquad \text{(A8)}$$

Inserting $d\eta_1 = \lambda_1 d\xi_1$ ($\lambda_1 = d\eta_1 / d\xi_1$) in (A8), we obtain

$$d\xi_1^2\, a_{11} + 2\lambda_1 d\xi_1^2\, a_{12} + \lambda_1^2 d\xi_1^2\, a_{22} = 1 \qquad \text{(A9)}$$

which gives

$$d\xi_1 = \frac{1}{(a_{11} + 2\lambda_1 a_{12} + \lambda_1^2 a_{22})^{1/2}} \qquad \text{(A10)}$$

and $d\eta_1$ is given by

$$d\eta_1 = \lambda_1\, d\xi_1 \qquad \text{(A11)}$$

In the same way, considering $i = j = 2$ in (A7), we obtain

$$d\xi_2 = \frac{1}{(a_{11} + 2\lambda_2 a_{12} + \lambda_2^2 a_{22})^{1/2}} \qquad \text{(A12)}$$

and $d\eta_2$ is given by

$$d\eta_2 = \lambda_2\, d\xi_2 \qquad \text{(A13)}$$

Finally the principal directions of curvature are obtained as [2]

$$\begin{aligned} \boldsymbol{a}_{P1} &= \boldsymbol{a}_1\, d\xi_1 + \boldsymbol{a}_2\, d\eta_1 \\ \boldsymbol{a}_{P2} &= \boldsymbol{a}_1\, d\xi_2 + \boldsymbol{a}_2\, d\eta_2 \end{aligned} \tag{A14}$$

Again the principal directions are orthogonal, so that

$$\boldsymbol{a}_{P1}.\boldsymbol{a}_{P2} = \left[d\xi_1\,, d\eta_1\right][a]\begin{bmatrix} d\xi_2 \\ d\eta_2 \end{bmatrix} = 0 \tag{A15}$$

and

$$\boldsymbol{a}_{P1}.\boldsymbol{a}_{P1} = 1 \qquad \text{and} \qquad \boldsymbol{a}_{P2}.\boldsymbol{a}_{P2} = 1 \tag{A16}$$

Principal stress directions

The principal stresses are given by

$$\sigma_{1,2} = \frac{1}{2}(\sigma_{xx} + \sigma_{yy}) \pm \frac{1}{2}\left[(\sigma_{xx} - \sigma_{yy})^2 + 4\,\sigma_{xy}^2\right]^{1/2} \tag{A17}$$

The angle between the first principal stress axis and the first local axis (see Figure A4) is given by

$$cos(2\alpha) = \frac{\frac{1}{2}(\sigma_{xx} - \sigma_{yy})}{\left[\left[\frac{1}{2}(\sigma_{xx} - \sigma_{yy})\right]^2 + \sigma_{xy}^2\right]^{1/2}} \tag{A18}$$

The principal stress directions are obtained as [3]

$$\begin{aligned} \boldsymbol{a}_{S1} &= \quad \boldsymbol{t}_1\, cos(\alpha) + \boldsymbol{t}_2\, sin(\alpha) \\ \boldsymbol{a}_{S2} &= -\boldsymbol{t}_1\, sin(\alpha) + \boldsymbol{t}_2\, cos(\alpha) \end{aligned} \tag{A19}$$

Finally a dot product between the first stress principal direction and the first principal curvature direction is performed to find out whether these two directions are aligned or normal to each other

---

[2] $\boldsymbol{a}_1$ and $\boldsymbol{a}_2$ are shown in Figure A1 and A2.

[3] $\boldsymbol{t}_1$ and $\boldsymbol{t}_2$ are shown in Figure A4.

- When these two directions are aligned then the formulae derived so far for the critical stresses for instance do apply as such *i.e.*

$$\sigma_1^{cr} = \sigma_1^{cr}(1/R_2) \qquad \text{and} \qquad \sigma_2^{cr} = \sigma_2^{cr}(1/R_1) \tag{A20}$$

- When these two directions are normal to each other, then the radii of curvature used in the computation of the critical stresses should be swapped as follows

$$\sigma_1^{cr} = \sigma_1^{cr}(1/R_1) \qquad \text{and} \qquad \sigma_2^{cr} = \sigma_2^{cr}(1/R_2) \tag{A21}$$

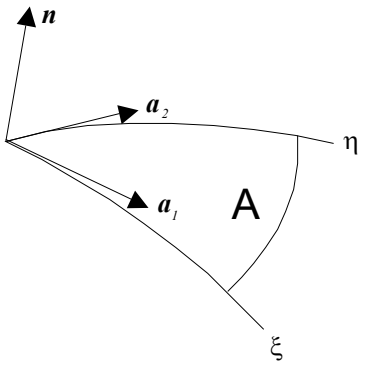

Figure A1 : Unit normal and tangent vectors on a shell surface.

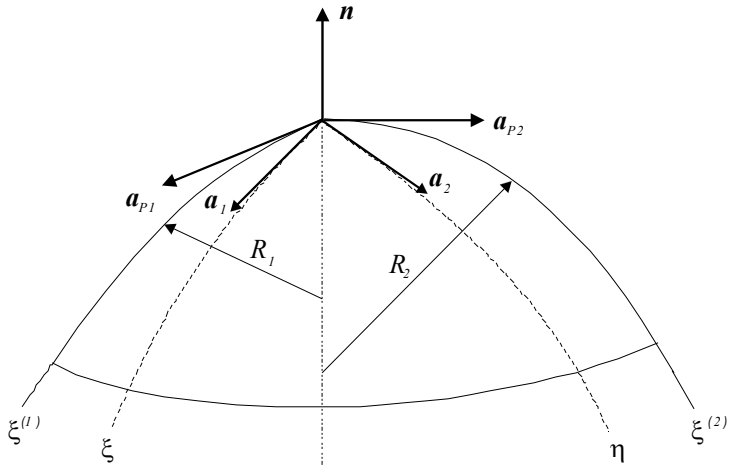

Figure A2 : Principal curvature directions.

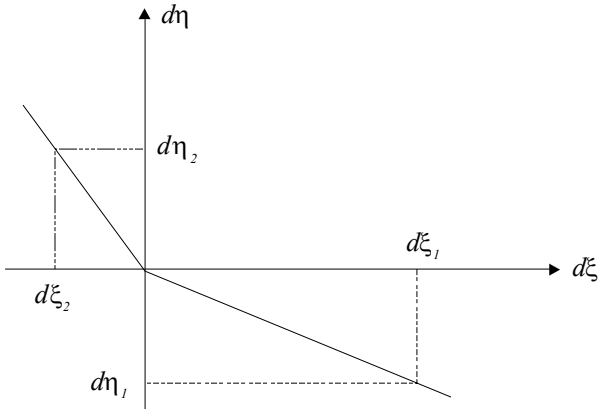

Figure A3 : (ξ,η) – Space.

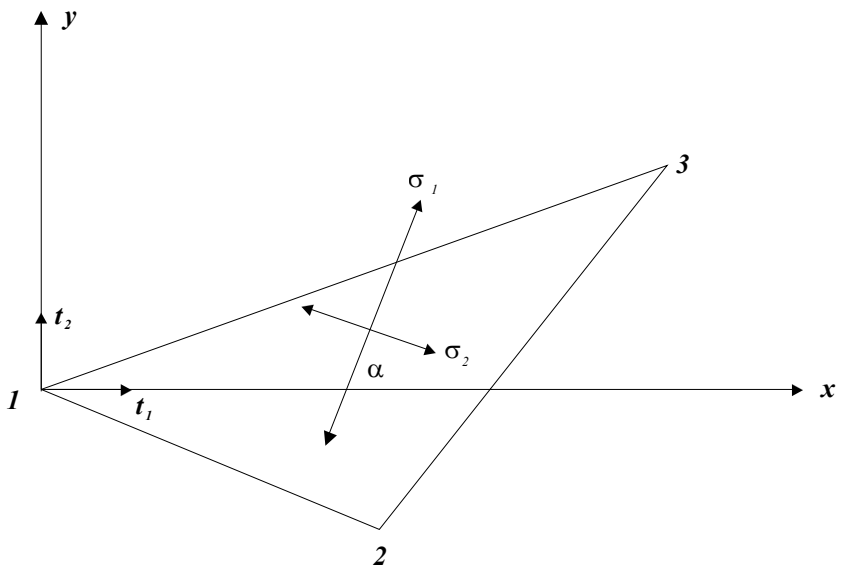

Figure A4 : Principal stress directions.